Materials Research Express

PAPER • OPEN ACCESS

Microstructure and mechanical properties of Cu-ZTA cermet prepared by vacuum hot pressing sintering

To cite this article: Da-Ming Sun *et al* 2020 *Mater. Res. Express* **7** 026530

Materials Research Express

OPEN ACCESS

RECEIVED
20 October 2019

REVISED
5 January 2020

ACCEPTED FOR PUBLICATION
15 January 2020

PUBLISHED
10 February 2020

PAPER

Microstructure and mechanical properties of Cu-ZTA cermet prepared by vacuum hot pressing sintering

Da-Ming Sun[1,2], **Xiao-song Jiang**[1,2], **Hong-liang Sun**[1,2], **Ting-feng Song**[3] and **Zhi-ping Luo**[4]

[1] Key Laboratory of Advanced Technologies of Materials, Ministry of Education, Chengdu 610031, People's Republic of China
[2] School of Materials Science and Engineering, Southwest Jiaotong University, Chengdu Sichuan 610031, People's Republic of China
[3] Institut de Ciència de Materials de Barcelona (ICMAB-CSIC), Campus UAB, Bellaterra 08193, Barcelona, Spain
[4] Department of Chemistry and Physics, Fayetteville State University, Fayetteville, NC 28301, United States of America

E-mail: xsjiang@swjtu.edu.cn

Keywords: powder metallurgy, vacuum hot pressing sintering, cermet, interface bonding

Abstract

In this paper, seven copper-zirconia toughened alumina (Cu-ZTA) cermets were prepared by vacuum hot pressing sintering (VHP). The effects of different binder content and different particle size of ZTA particles on the mechanical properties of Cu-ZTA cermets were investigated. The microstructure of the composites was studied by x-ray diffraction, scanning electron microscopy and energy dispersive spectroscopy. The hardness of the material was measured by micro Vickers hardness tester. The results show that the solid solution strengthening occurs in the hot pressing sintering process, the formation of copper-based solid solution increases the hardness of the matrix, the highest is 192.04 $HV_{0.1}$. The ZTA particles are uniformly distributed in the matrix, and the surface of the ZTA particles is surrounded by a continuous coppermatrix and second phase. Two interfaces are formed between ZTA particles and Cu matrix. One is the ZTA/Cu interface formed by the substitution of Cu atoms for Ni atoms, it is a mechanical meshing interface which extends the service life of cermet under mechanical stress and thermal stress. The other interface is the reaction bonding interface of Cu_3Ti_3O and TiO_x. The friction and wear test results show that the use of low-diameter ZTA particles and increasing the content of Cu binder will improve the friction and wear properties of Cu-ZTAcermet. Under the action of stress, the fracture occurs at the interface of Cu/ZTA, and the wear, fracture and extraction of ZTA ceramics cause the failure of Cu-ZTA cermet.

1. Introduction

Cermets are widely used in cutting tools due to their excellent mechanical properties [1–5]. Cermets have high bonding strength, good formability, strong abrasiveness and can withstand large loads during processing [1, 6–8]. At present, cermet substrates are often made of metals such as Al, Cu and Fe. Among them, metallic copper has been widely used in the preparation of cermets due to their low cost, excellent electrical, thermal and mechanical properties [9–13]. Cu-based cermets with ZTA [14–16], TiC [3, 16], WC [2, 17], TiB_2[10] and other reinforcing phases have significant advantages over pure metals. The cermet material with ZTA as the reinforcing phase has excellent toughness of metal materials and has excellent wear resistance and chemical stability of ceramic materials [18]. The ZrO_2 contained in ZTA undergoes a transition from tetragonal to monoclinic when subjected to stress, which consumes the energy of crack propagation and thus improves the toughness of Cu-ZTA cermet [9]. Hence, ZTA is an ideal material for the preparation of cermets [16].

In recent years, the interfacial bonding strength and interfacial bonding mechanism between ZTA and metals have been extensively studied [15, 19, 20]. Al_2O_3 and ZrO_2 are polar materials, so it is hard to bond with metals, which limits the bonding ability between ZTA and metals [20]. To solve this problem, ZTA needs to be surface treated. The common surface treatment methods include spraying [21, 22], electroless plating [20, 23, 24], chemical vapor deposition (CVD) [25, 26], ion beam sputtering [27], etc. Studies have shown that electroless plating is an effective way to improve the bonding ability of ZTA and metals [28, 29]. Electroless

Table 1. Composition of Cu-ZTA cermet (wt%).

Number	Copper binder	ZTA	FeS_2	Na_3AlF_6	TiH_2	$CaCO_3$	La	Cr	graphite	WC	Remarks
F10-1	30	52.5	2.5	2.5	3	2	0.5	1	1	2.5	
F10-2	35	50	2.5	2.5	3	2	0.5	1	1	2.5	
F10-3	40	45	2.5	2.5	3	2	0.5	1	1	2.5	
F10-4	35	50	2.5	2.5	3	2	0.5	1	1	2.5	Electroless plating
F10-5	40	45	2.5	2.5	3	2	0.5	1	1	2.5	Electroless plating
F14-2	40	45	2.5	2.5	3	2	0.5	1	1	2.5	Electroless plating
F14 + 16-1	35	25/25	2.5	2.5	3	2	0.5	1	1	2.5	Electroless plating

nickel plating can effectively control the thickness of the coating and is widely used for surface modification of ceramic materials [30, 31]. Juan *et al* [8] found that after nickel plating on the surface of ZTA, Ni and Al reacted and wetted at the interface under high temperature condition, which improved the wettability of Al and ZTA. Ru *et al* [15] found that Ni-coated ZTA particles can wet with Fe matrix at high temperatures because Ni atoms diffuse into the Fe matrix in the presence of liquid phase. The liquid metal penetrates in the dimples and pores of the ceramic surface by capillary force to form a dense structural layer, which improves the interfacial bonding strength. Considering that Cu and Ni can form a solid solution [32], electroless nickel plating is expected to be a method for improving the wettability between ZTA and Cu [32]. In addition to improving the wettability of the interface, a suitable sintering process can also improve the interfacial bonding ability of ZTA and Cu. In the method of preparing copper-based cermet, powder metallurgy has become the first choice for the high density and low cost of the prepared cermet [1, 33, 34]. Vacuum hot pressing (VHP) is a manufacturing process for manufacturing cermets [18]. Ji *et al* [35] used VHPs to prepare Ni-bonded Ti(C, N)-based cermets. Due to diffusion, Ti(C, N) grains dissolved in the Ni matrix to form edge phases that improved the wettability between binder and ceramics.

At present, there are few studies on Cu-based cermets with ZTA as the reinforcing phase, its mainly because the poor interfacial bonding ability between ZTA and Cu. The mismatch of coefficient of thermal expansion (CTE) between ZTA and Cu also influence the use of Cu-ZTA cermet. Therefore, in this paper, the metal Cu is used as the binding agent innovatively. The alloy element,such as Ni, can not only strengthen the solid solution, but also balance the CTE difference between ZTA and Cu. The surface of ZTA particles is plated with Ni to improve the bonding ability with Cu. Finally, Cu-ZTA cermet was prepared by VHPs. The effect of nickel plating on the wettability of ZTA and Cu matrix and the effect of ZTA particle size on the mechanical properties of Cu-ZTA cermet were evaluatedby testing the mechanical properties of Cu-ZTA cermet. Based on the experimental results, the formation mechanism of Cu/ZTA interface and the friction and wear mechanism of Cu-ZTA cermets were discussed.

2. Experimental

2.1. Materials and composites fabrication

In this paper, seven different Cu-ZTA cermets with different binder contents and different ZTA particle sizes were prepared. The ZTA particle diameters used in this paper were 2.00 mm (F10), 1.40 mm (F14), and 1.18 mm (F16), respectively. The metal binder is a mixture of copper, tin, nickel and zinc, the mass ratio is 85:6:5:4. The Cu-ZTA cermet substrate is reinforced by FeS_2, Na_3AlF_6, TiH_2, $CaCO_3$, Cr, La, graphite and WC. The specific parameters are shown in table 1.

The flow chart is shown in figure 1. Raw materials were placed in a planetary ball mill (WL-1) and wet-milled with the speed of 200 r min^{-1} for 2 h, the wet-milling medium was t-butanol. After the completion of the ball milling, the mixed powder was placed in a freeze dryer (FD-A-50) and dried for 24 h. The raw materials are sintered by vacuum hot pressing (VHP, HAS-25). The sintering temperature was 900 ° C with the pressure of 12 MPa, the holding time was 120 min. Then the grinding test of Cu-ZTA cermets was carried out. The grinding test of the U17Mn steel bar was tested by a self-made grinding test stand. The grinding speed is 600 r min^{-1} and grinding pressure is 500 N. The chemical composition of the steel bar is shown in table 2.

2.2. Characterization of composites

The microstructures of the composite powders and bulk composites were examined and analyzed by scanning electronmicroscope (SEM, Hitachi S-4800) equipped with EDS and x-ray diffraction analysis(XRD, X. Pert Pro-MPD). The hardness of the Cu-ZTA cermets substrate were tested by digital micro-Vickers hardness tester (HVS-30). The friction coefficient and surface roughness of the friction interface between Cu-ZTA cermet and steel bars were measured by the self-made equipment. The grinding ratio of several kinds of cermet to steel bars

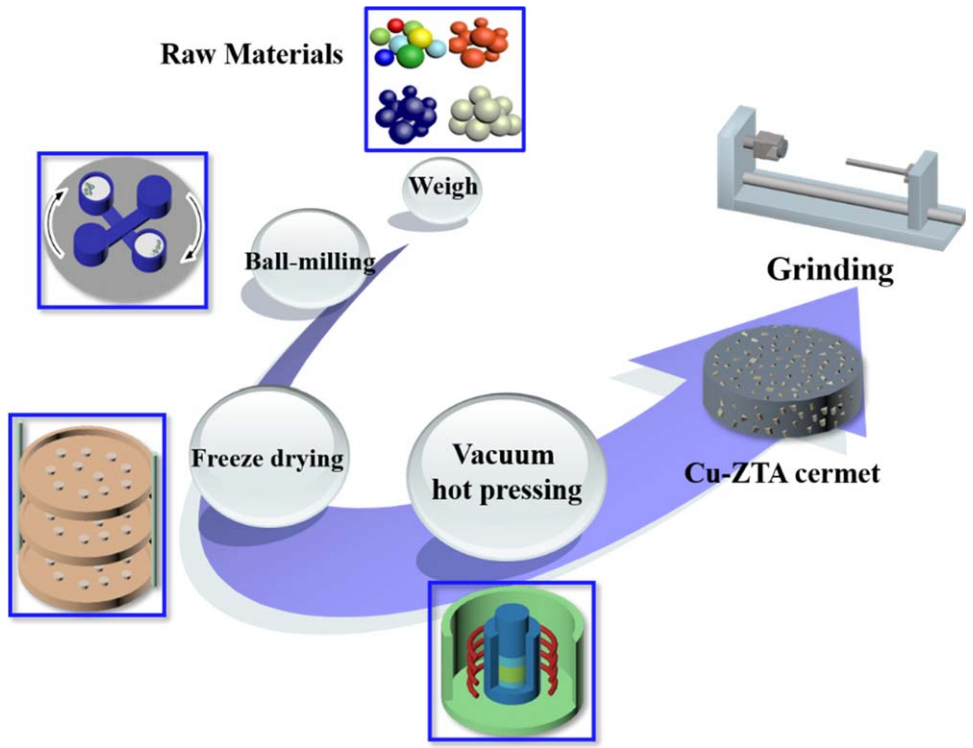

Figure 1. Flow chart of preparation of Cu-ZTA cermet.

Table 2. The chemical composition and physical properties of the rail material [36].

Chemical composition	Steel bars	C	Si	Mn	S	P	V	Nb
	U17Mn	0.65–0.76	0.15–0.35	1.10–1.40	⩽0.030	⩽0.030	⩽0.030	⩽0.010
Physical properties	Steel bars	Tensile strength σb (MPa)		Elongation rate δ (%)		Shrinking rate ψ (%)		Hardness ($HV_{0.05}$)
	U17Mn	⩾900	⩾10	⩾14	290			

was tested to characterize the grinding ability of Cu-ZTA cermet. The morphology of the worn steel bar was analyzed by scanning electron microscopy (SEM, Hitachi S-4800).

3. Results and discussion

3.1. Electroless nickel plating of ZTA particles

In order to study the combination of ZTA particles and copper matrix after electroless nickel plating, the morphology of ZTA particles were observed by SEM. Figures 2(a) and (b) show ZTA particles which have not been electroless plated with nickel. It can be found that the surface of the ZTA particles is uneven, which reducing the binding ability of the ZTA particles to the metal matrix. The EDS spectrum results confirm that the material at points 1–3 in figure 2(b) is ZTA that composed of ZrO_2 and Al_2O_3. Compared with figures 2(a) and (c), the surface of the ZTA particles after electroless nickel plating is flat. It can be observed from figures 2(c) and (d) that after electroless nickel plating, the surface of the ZTA particles become relative flat because the electroless nickel plating has the characteristics of uniform plating thickness [30, 31]. After electroless nickel plating, the pores on the surface of ZTA are covered by Ni to form a uniform thickness of nickel layer that enhance the binding ability of ZTA to copper-based binders. The EDS spectrum results show that the nickel content at point 5 is almost zero. The elemental contents of Al and Zr are consistent with ZTA ceramics, indicating that the nickel plating layer is broken at point 5, the inside of the notch is ZTA particles. Figure 2(d) show that the thickness of the electroless nickel layer is substantially the same. The energy spectrum at points 4 and 6 confirmed that the surface electroless plating of the ZTA particles was a nickel layer.

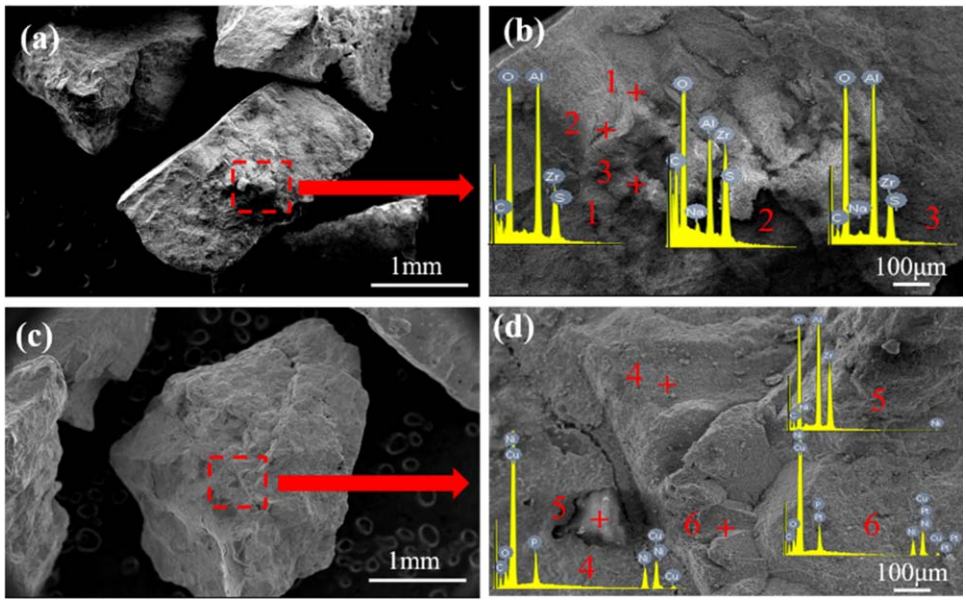

Figure 2. Scanning electron micrograph of ZTA particles (a)–(b) ZTA particles without electroless plated (c)–(d) ZTA particles after electroless plating.

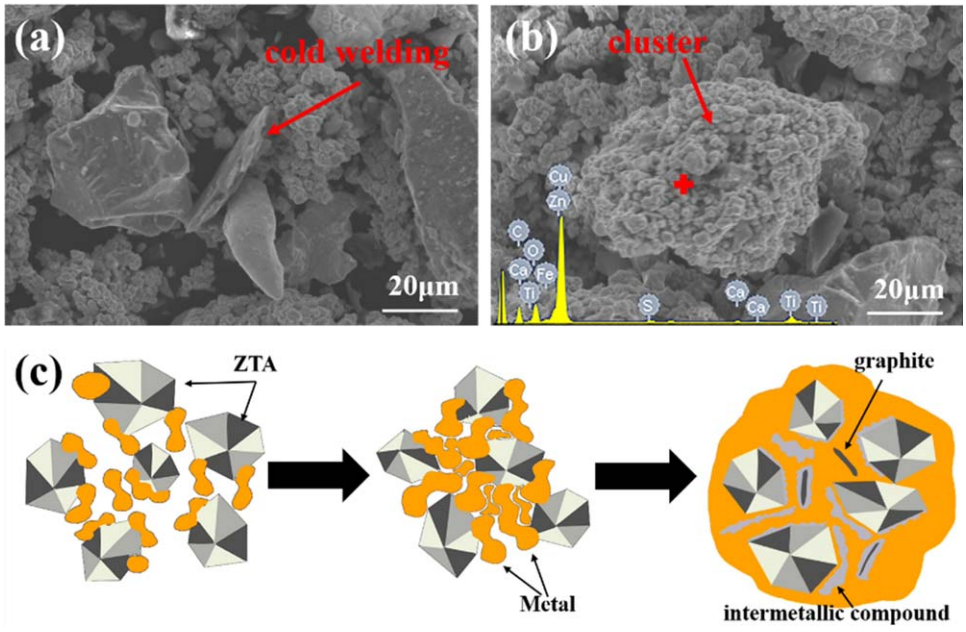

Figure 3. (a)–(b) SEM image of Cu-ZTA cermets composite powders of F10-5 sample; (c) sintering process diagram of Cu-ZTA cermets prepared by hot-pressing process.

3.2. Preparation of Cu-ZTA cermet

Mechanical alloying is an important method for strengthening Cu-based composites [37–39]. Figures 3(a) and (b) show the SEM images of Cu-ZTA cermet powder. The phenomenon of cold welding of copper powder is shown in figure 3(a). In the process of mechanical ball milling, the copper powder and other alloying element powders are plastically deformed and broken under the action of external force, and the size of the raw material powder reduced. The copper particles and other alloy elements are combined into a cluster during continuous stirring [33], the EDS results demonstrate that the cluster particles are composed of various elements (figure 3(b)). Mechanical alloying can also achieve interatomic bonding between the various metal powder [39]. Studies have shown that speed up the ball milling speed and delay the ball milling time can reduce the size of the raw materials to make the reinforcing phase more evenly distributed, and improve the combination of each component [40, 41]. At the same time, the broken copper particles are cold welded during mechanical ball

milling [41, 42]. After the ball milling, the surface of the ZTA particles will adhere to the metal binder that promotes ZTA bond tomatrix.

Figure 3(c) is a schematic view of the sintering process of Cu-ZTA cermet. Under a condition of 900 °C and 12 MPa, the elements such as Zn, Ni, and Sn in the matrix are solid-dissolved into the Cu matrix to form a solid solution and increase the strength of the Cu-ZTA cermet matrix. Then, the matrix starts to grow under heating conditions, filling the gap between the ZTA and the matrix, achieve the effect on the bonding of ZTA particles [43, 44]. As the temperature decreases, the growth process of the crystal grains is basically completed, and the matrix is composed of a copper-based solid solution, which accompanied by the formation of some intermetallic compounds. The graphite in the raw material is distributed in the copper-based solid solution, serves to strengthen the matrix and improve the lubricity of the material. In addition, studies have shown that due to the difference coefficient of thermal expansion between ZTA particles and residual stress is generated between metal binder and ZTA. In this paper, the addition of elements such as Ni, Sn and Zn can lower the melting point of the Cu-based metal bond, so that some liquid phase will appear during the heat preservation process. The relaxation of the stress is achieved by the diffusion flow mechanism [45] and the allotropy transformations of ZrO_2 in ZTA, thereby reducing the concentrated stress [46, 47].

3.3. Microstructure and phase of Cu-ZTA cermet

Cu-ZTA cermets with different ZTA contents have the same structure after vacuum hot pressing because of the same manufacturing process. The SEM images of the interface and substrate of F10-5 Cu-ZTA cermet are shown in figure 4. Figure 4(a) is the low magnification SEM image of the F10-5 Cu-ZTA cermets, the ZTA particles are evenly distributed in the Cu-ZTA cermet. Holes in the substrate are caused by polishing. A ZTA particle in figure 4(b) is completely covered by the matrix, the interface between Cu matrix and ZTA is tightly connected, and there are no obvious cracks. It can be seen from figure 4(c) that the ZTA particles are tightly bonded to the Cu matrix, and there are no cracks, pores and shrinkage in the matrix. No significant interfacial reaction was observed and the ZTA particles were mechanically meshed with the copper matrix. In figure 4(d), there is a loose interfacial layer between the ZTA and the substrate, and a dark gray phase can be clearly seen in the Cu matrix, it is speculated that the phase is an intermetallic compound. In figure 4(e), there are mainly three kinds of phases in the matrix: a white bulk phase, a black flake phaseand a discontinuous dark grey phase. Among them, the white area accounts for the largest proportion, and the black phase is embedded in it. It is presumed that the white phase is copper matrix, and the black phase is graphite. The dark gray phase formed between the substrate and the ZTA particles, since the phase is enriched near the graphite sheet and the boundary between the substrate and the substrate is irregular and unclear, so it is speculated that the dark gray phase is an *in-situ* intermetallic compound [48, 49]. In order to further elaborate the elemental composition of each phase, a dot scanning analysis was performed on several phases in figure 4(e), and the results are shown in table 3. It can be confirmed that the black and white regions in figure 4(e) are graphite and Cu, respectively, and the dark gray region is composed of some oxides.

The XRD pattern of F10-5 sample is shown in figure 4(f). The results show that the phase of the composite material changes significantly due to the diffusion of alloying elements during sintering. The diffraction peaks of elements such as Sn, La, Cr, S, and Na disappear, and it is presumed that these elements diffuse into the matrix to form solid solution or compound. In addition, XRD results show that Zn element is solid-dissolved into the Cu matrix to form Cu_3Zn solid solution, because high temperature and high pressure conditions provide sufficient power for atomic diffusion [50, 51]. The TiH_2 in the matrix will decompose under high temperature, and the Ti atoms generated after the decomposition will react with ZTA and the matrix to form TiO and Cu_3Ti_3O. The reaction equation is as shown in (1) [52], (2)–(3) [53]:

$$TiH_2 \rightarrow TiH_{1.5} \rightarrow Ti\ (\text{with H in solution}) \rightarrow Ti \quad (1)$$

$$Al_2O_3 + Ti = 2Al + 3TiO \quad (2)$$

$$Al_2O_3 + 3Cu + 5Ti = Cu_3Ti_3O + 2TiO + 2Al \quad (3)$$

$$\Delta G = 526.58 - 0.554T(K)$$

In the process of vacuum hot pressing sintering, TiH_2 decomposed and the Ti element react with Al_2O_3 to form Al and TiO (equation (2)). The Cu-ZTA cermet produced in this paper is similar to weld ZTA to Cu substrate. ZTA contains alumina and zirconia, Ti element can improve the wettability between Cu and Al_2O_3 to form $Ti_3(Cu, Al)_3O$ (M_6O-type) compound [54, 55] and form ZrO_{2-x} and xTiO with ZrO_2 [56] at the interface. As the content of Ti element changes, the composition of this M_6O compound also changes. Under the conditions of the atomic ratio x_{Ti}/x_{Cu+Al} ratio (1.20 versus 1.05), Ti_3Cu_3O and Ti_2Cu_4O compounds are formed, respectively [54]. Both compounds containing some dissolved Al. Kozlova [57] *et al* found that low temperature conditions ($T \leqslant 820$ °C) and titanium content higher than 3 wt% can lead to the formation of the intermetallic compound Ti_3Cu_3O. In this paper, the atomic ratio$x_{Ti}/x_{Cu+Al} \approx 1.53$ at the interface, and the

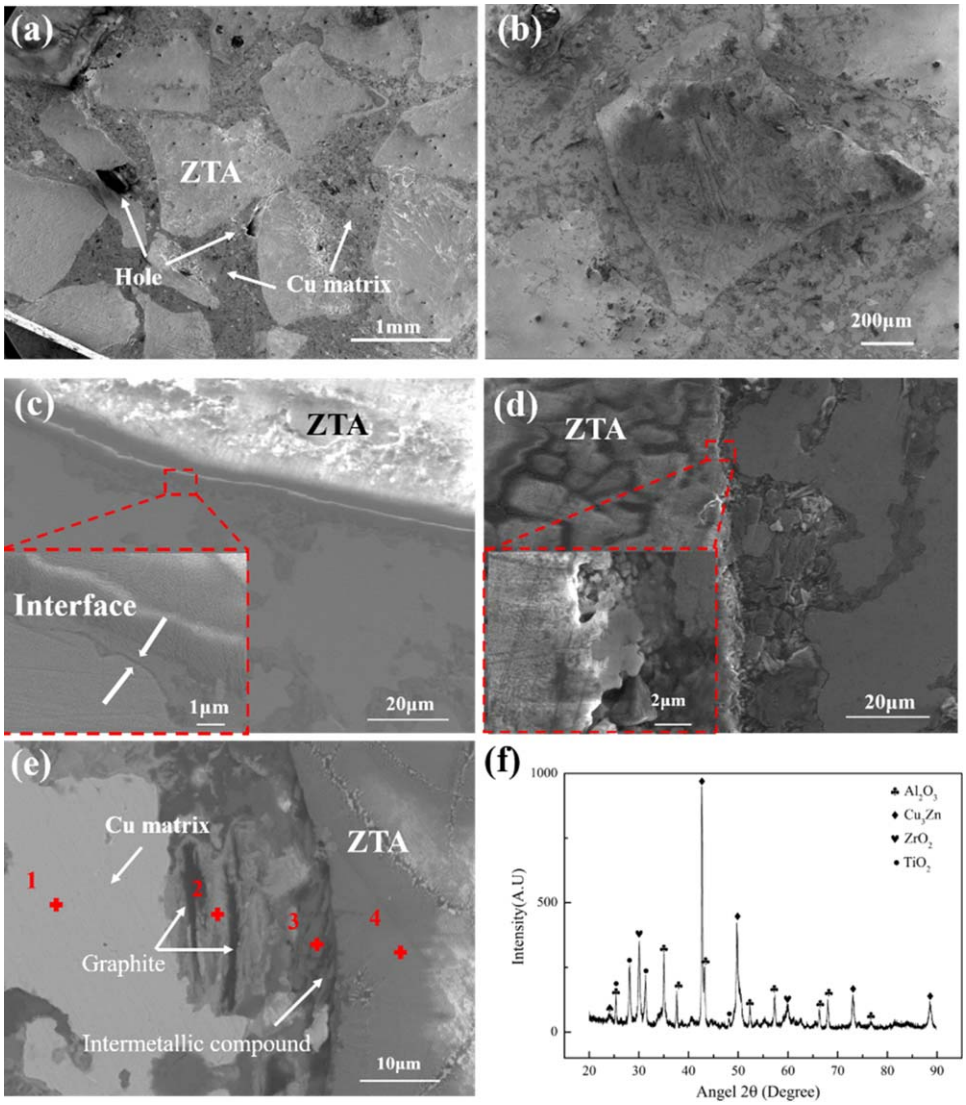

Figure 4. (a)–(b) Low magnification SEM image of the F10-5 Cu-ZTA cermets; (c)–(e) SEM image of interface between ZTA and Cu matrix of F10-5 sample; (f) XRD pattern of F10-5 sample.

Table 3. Energy spectrum results at each point in figure 4(c) (at%).

	C	O	Cu	Ti	Al	Na	F	Ca	S	Fe	Cr	Zr	Zn	Ni	Sn	La
1	18.4	—	68.9	—	—	—	—	—	—	1.4	—	—	5.4	4.1	1.8	—
2	35.1	44.4	6.5	0.5	1.9	6.8	3.0	1.2	0.2	—	—	—	—	—	—	—
3	40.2	19.8	8.9	13.6	—	—	—	—	9.2	2.4	5.3	—	—	—	—	0.4
4	11.3	54.4	—	—	25.5	1.5	1.4	0.2	—	—	—	5.8	—	—	—	—

excess Ti element exists as a oxide of TiO_x. At 900 ° C, the Gibbs free energy of formula (3) is $\Delta G = -123.35$ kJ mol^{-1}, so that the reaction can take place during vacuum hot pressing.

Figure 5 shows the surface scanning results of the F10-5 sample. It can be seen from figure 5(a) that an interface layer exists between the copper matrix and ZTA. Figures 5(b)–(d) show that the ZTA is mainly composed of Zr, Al, and O elements. As shown in figures 5(d), (g), (k), (l), there are O, S, F, Ti element enrichment at the interface and the substrate, it might have formed solid solution. These other phases are not found in the XRD results due to limitations in XRD measurement accuracy. Figure 5(e) shows that the matrix is mainly composed of Cu elements, in which some alloy elements such as Sn, Zn, Ni are solid-solved [48]. In figure 5(i), the Ni element is uniformly distributed in the matrix region due to the addition of Ni to the matrix Cu. However, no obvious Ni-rich layer was found at the ZTA/Cu interface, indicating that the Ni layer on the surface of the ZTA particles diffused into the matrix during vacuum hot pressing. Ni plating can only increase

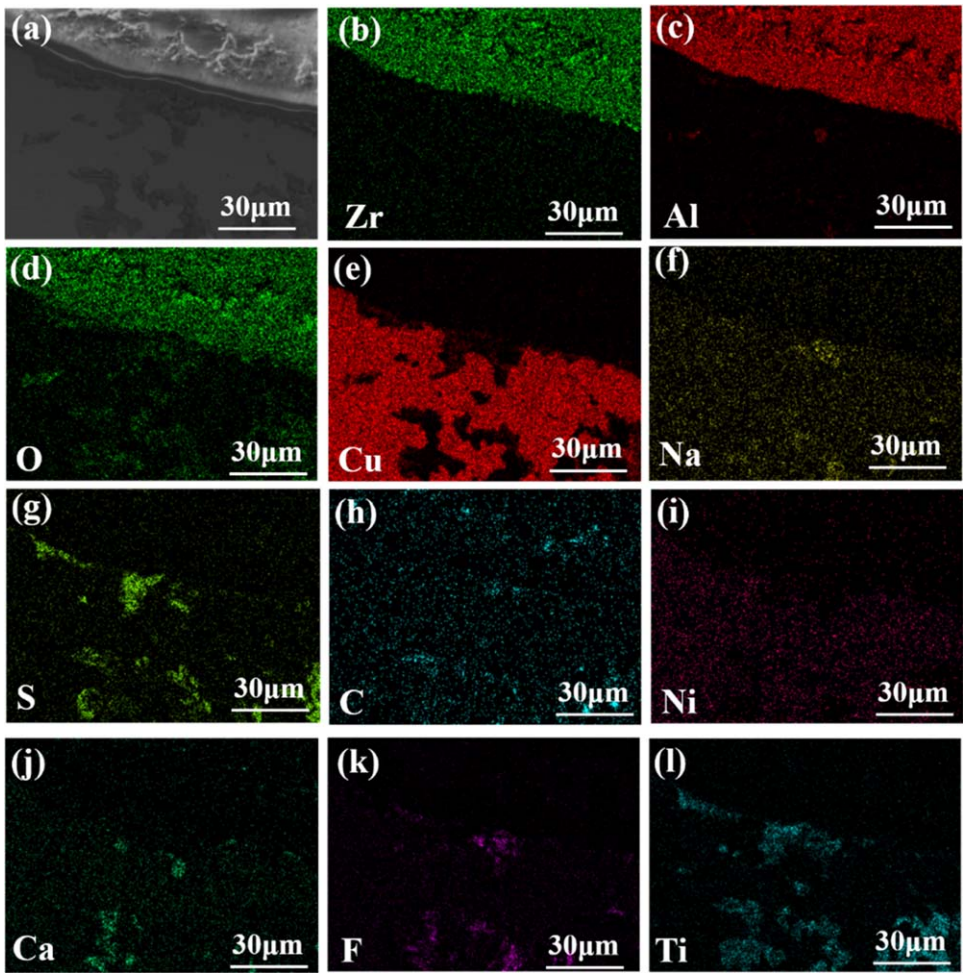

Figure 5. (a) SEM images of the matrix and (b)–(i) distribution of elements across the Cu-ZTA cermet.

the bonding ability between ZTA particles and matrix than to achieve chemical bonding between metal and ceramic [14], which also confirms the conclusion of mechanical bonding between ZTA and Cu matrix.

Combined with the results of EDS and XRD, conclusion can be drawn that the Cu_3Zn solid solution is formed in the Cu matrix to strengthen the matrix. There are also other phases formed inside the matrix, the main phase is TiO_x. The loose interfacial layer formed at the interface between the substrate and ZTA. Based on the point scanning results and thermodynamic calculations, the intermetallic compound Cu_3Ti_3O and oxide TiO_x are formed at the interface.

3.4. Formation mechanism of Cu/ZTA interface

Interfacial bonding state is a major factor in determining the strength of cermets. Therefore, exploring the interface formation mechanism between ZTA and Cu helps to understand the strengthening mechanism. In figures 4(a) and (b), it is found that there are two kinds of interface between ZTA and Cu matrix, one interface is mechanical bonding between Cu and ZTA, and the other is a reaction bonding interface. The schematic diagram is shown in figure 6. At the initial stage of vacuum hot press sintering, there is a gap between the ZTA and the Cu matrix, and the ZTA surface is evenly butchered with a layer of Ni (figure 6(a)). Copper particles deformed and melted under high temperature and load conditions, the melted liquid phase fills the gap between ZTA and Cu. Simultaneously, Ni atoms on the surface of the ZTA gradually diffuse into the Cu matrix, and the vacancies formed by the diffusion of the Ni atoms are filled with Cu atoms. The bonding between Cu and ZTA particles can be achieved during the atomic substitution process to form a good ZTA/Cu interface (figure 6(b)). Ni atoms diffused into the matrix can form a solid solution with Cu, increasing the strength of the matrix [32]. As shown in figure 6(c),Al_2O_3 in the ZTA particles reacts with Ti and Cu to form Cu_3Ti_3O and TiO_x, and finally forms the interface of ZTA/Cu_3Ti_3O/Cu and ZTA/TiO_x/Cu. By analyzing the interface distribution between ZTA and Cu matrix, the friction performance of Cu-ZTA cermet can be better analyzed.

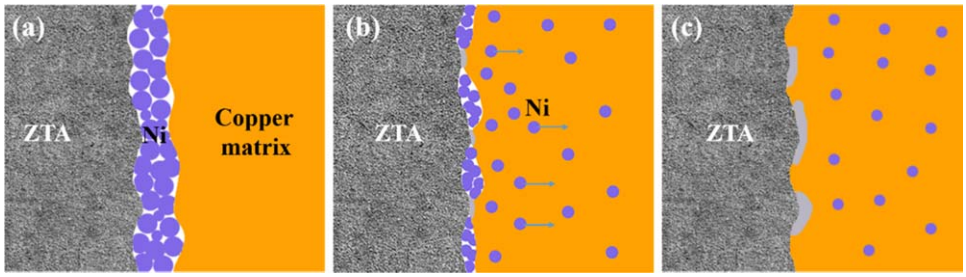

Figure 6. Schematic diagram of the interface between ZTA and Cu.

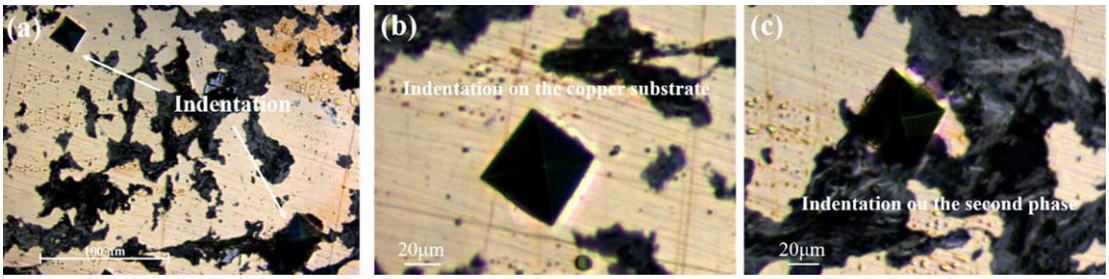

Figure 7. (a) OM images of Cu-ZTA cermet using ZTA particle size of F14 + 16−1 and Micro Vickers hardness tester indentation (b) on the copper substrate (c) on the second phase.

3.5. Hardness of Cu-ZTA cermet

Cu-ZTA cermets with different ZTA contents have the same structure after vacuum hot pressing because of the same manufacturing process. Therefore, the difference in hardness between individual samples is negligible. Figure 7 are OM images of Cu-ZTA cermet using ZTA particle size of F14 + 16−1. It can be seen from figure 7(a) that there are indentations on the copper substrate and second phase. The indentation area on the second phase is larger than the area on the copper substrate. Figure 7 (b) shows the micro Vickers hardness indentation on the copper substrate. The average value of the micro Vickers hardness was 192.04 (±14) $HV_{0.1}$. Compared with pure copper (50 ∼ 65 HV) and other copper alloy (70 ∼ 130HV), the hardness of the cermet substrate is greatly improved. The reason is that the alloying elements Ni, Sn, and Zn are added in the matrix and these elements can form a solid solution during VHPs [58, 59]. In addition, graphite is added into the raw material, and the diffusion of C element into the matrix can increase the hardness of the matrix. When measuring the hardness of the Cu-ZTA cermet matrix, the indenter of the micro Vickers hardness tester also forms an indentation at the second phase in the Cu matrix (figure 7(c)). The EDS spectrum in figure 5 shows that these second phases are mostly composed of oxides and carbides. These second phases have a micro Vickers hardness of 172.26 (±15) $HV_{0.1}$, which is lower than the hardness of the matrix. It is precisely because of the existence of the second phase which is discontinuously generated at the interface and the substrate. During the grinding process, cracks are first generated on these fragile second phases and then diffused into the matrix. The ZTA particles can be discharged from the friction pair in time to improve the service life of the cermet material.

3.6. Grinding behavior of Cu-ZTA cermets

The SEM images of the surface morphology of steel bars grinded by seven Cu-ZTA cermets are shown in figures 8(a)–(d). The steel bar is a tough material and the material is removed by plastic flow during the grinding process. It can be seen from figures 8(a) and (b) that there are grinding grooves on the surface of the steel bars and the presence of axial furrows in some areas. The wear scar distribution in figure 8(b) is relatively uniform and the grinding groove is shallow. There are two reasons for this phenomenon: 1. Due to the low content of Cu binder of F10-4 Cu-ZTA cermet, the coating ability of Cu bond to ZTA particles is weakened, ZTA particles protrude on the surface of Cu-ZTA cermet, partially over-exposed ZTA leaves a deeper grinding groove during the grinding process. 2. After electroless nickel plating, the interface bonding ability between ZTA and Cu matrix improved, some of the ZTA particles in the F10-4 Cu-ZTA cermet were damaged, and were not peeled off from the Cu matrix in time, so it is difficult to reveal ZTA particles [60], these broken abrasive particles will also have a bad influence on the grinding surface. In addition, oxidation and carbon deposition appear on the surface of the steel bar during grinding [61].

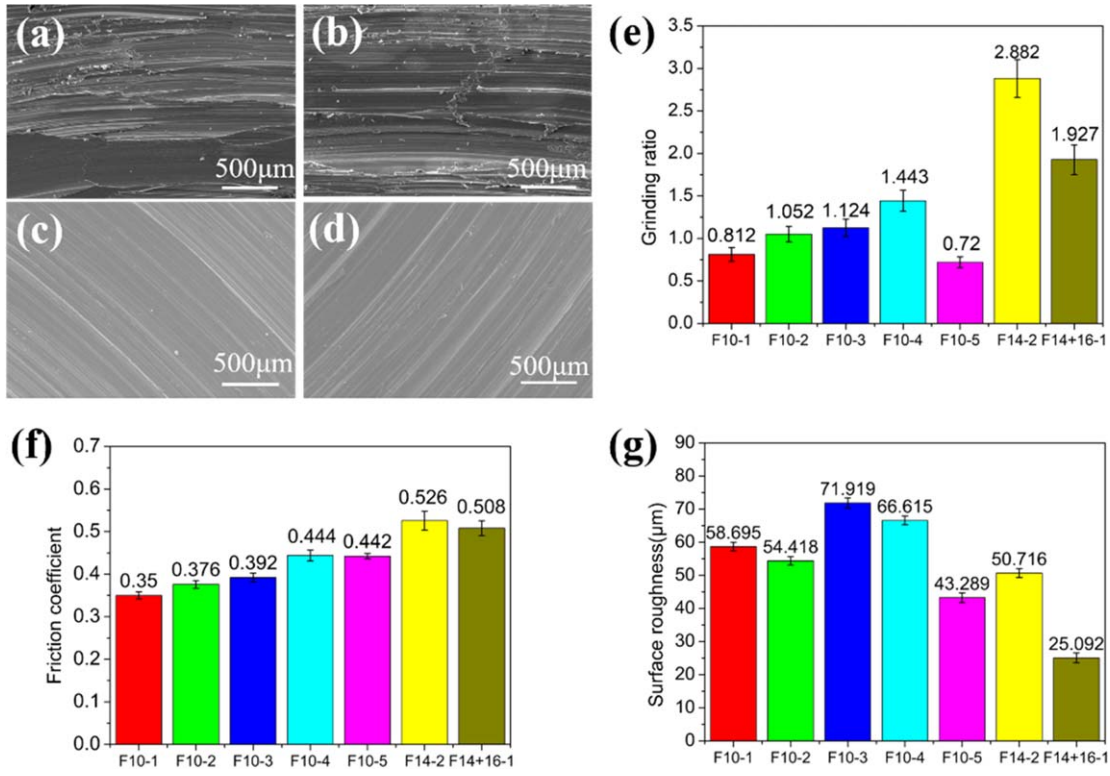

Figure 8. Surface morphology of steel bars after grinding with different types of Cu-ZTA cermets (a) F10-4; (b) F10-5; (c) F14-2; (d) F14 + 16−1 and (e) The abrasion loss of Cu-ZTA cermet to steel bars; (f) Friction coefficient of friction pair between Cu-ZTA cermets and steel bars; (g) Surface roughness of steel bars after grinding with cermet.

Figures 8(c) and (d) are SEM images of the wear surface of the steel bar ground by F14-2 and F14 + 16−1 Cu-ZTA cermets. It can be seen from the figures 8(c) and (d) that there is no deep grinding groove on the surface of the steel bar, the grinding cracks are uniformly distributed. Some plastic deformation areas are generated on the surface of the steel bar. These results show that the surface of the steel bar after grinding with low-grained Cu-ZTA cermet has excellent surface quality.

Grinding ratio (G) is an important index to measure the grinding performance of materials. The grinding ratio of materials is calculated by formula (4)

$$G = V_{wc} / V_{sc} \tag{4}$$

Where, V_{wc} is the volume of the work piece removed, V_{sc} is the loss volume of the grinding wheel, and G is the grinding ratio.

During the grinding process, not only the ZTA abrasive is worn, but also the matrix wear will occur. Because the density of ZTA abrasives and the density of the base material are different, it is difficult to quantitatively analyze the volume loss of cermets during grinding. Therefore, for formula (4), the value of Vsc cannot be quantitatively analyzed. Therefore, in this manuscript, V_{wc} was used to characterize the grinding ratio of Cu-ZTA cermets, only for comparison of the grinding performance of the seven Cu-ZTA cermets in this manuscript. In this paper, the V_{sc} is regarded as a constant of 1, so the grinding ratio of seven cermets on the steel bars under the same experimental conditions is shown in figure 8(e). It can be seen from figure 8(e) that when the unelectroless ZTA particles are used, the abrasion loss of the steel bars increases with the decrease of ZTA content. When electroless ZTA particles are used, the abrasion loss of steel bars decreases with the decrease of ZTA content. The reason is that the bonding strength between unelectroless ZTA and Cu matrix is weak. The Cu binder cannot tightly wrap too many ZTA particles, and too much ZTA may flake off in the grinding process and damage the processed surface (figures 8(a) and (b)). After electroless nickel plating on ZTA, Cu-ZTAcermet has a higher abrasion loss on the steel bars. This is because the interface bonding strength between electroless ZTA and Cu is better. In the grinding process, more ZTA is in contact with the contact surface, and the abrasion loss on the steel bars increase. Moreover, ZTA is not easy to peel because of its good bonding strength. When the particle size of ZTA is reduced, the abrasion loss of Cu-ZTA cermets on the steel bars increases, the reason is that the particle size of ZTA decreases and more ZTA is distributed at the grinding interface, so the abrasion loss on the steel bars increases [62].

Figure 8(e) shows the friction coefficient of the seven Cu-ZTA cermet friction pairs studied in this paper. Compare the friction factors of F10-1, F10-2 and F10-3 Cu-ZTA cermets. When electroless ZTA particles are not

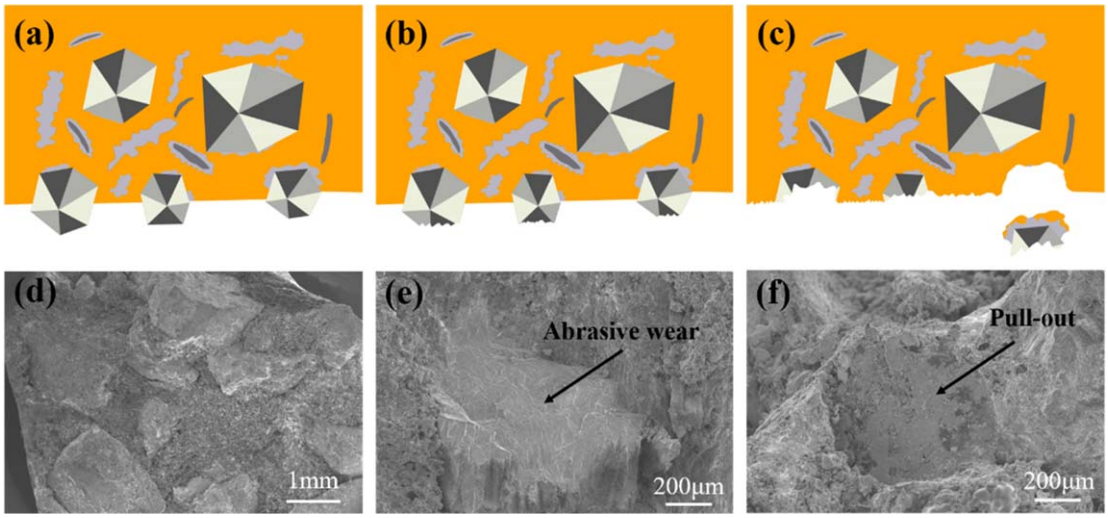

Figure 9. Schematic diagram and SEM imagesof the wear behavior of Cu-ZTA cermet during grinding (a), (d) Initial state; (b), (e) Abrasive wear of ZTA; (c), (f) Pull-out of ZTA abrasive.

used, the friction factor increases as the binder content increases because the binder can better coat the ZTA particles. When the F10-1 Cu-ZTA cermet is subjected to the grinding test, the ZTA particles are easily peeled off. Grinding occurs between the copper matrix and the steel bar, resulting in the lowest friction coefficient of the friction pair. The effects of electroless nickel plating on friction coefficient of friction pair were verified by comparing F10-2, F10-4 and F10-3, F10-5 Cu-ZTA cermets. It can be seen from figure 8(e) that the Cu-ZTA cermets using electroless nickel-plated ZTA has a high friction coefficient. This is because the ZTA particles after electroless nickel plating have strong interfacial bonding ability with matrix [14]. The excellent interface combination makes ZTA particles hard to fall off during grinding, which improved the grinding ability of Cu-ZTA cermet. Comparing the friction factor curves of F10-5, F14-2 sample and F10-4, F14 + 16−1 sample it can be found that when the particle size of the ZTA particles is reduced, the amplitude of the Cu-ZTA cermet friction factor decreases in the normal direction. The contact area of the Cu-ZTA cermets with the surface of the steel bars increases during the grinding process, and the abrasion loss of the steel bar increases. Therefore, under the same conditions, reducing the particle size of ZTA can increase the friction coefficient of the friction pair. This phenomenon is consistent with the results of Wang *et al* [62].

Figure 8(g) shows the surface roughness of the steel bars after grinded by seven Cu-ZTA cermets prepared in this paper. Samples F10-1, F10-2, F10-3 and F10-4, F10-5 were compared respectively to analyze the influence of binder content and ZTA electroless nickel plating treatment on the surface roughness of the steel bars. The results showed that when no nickel-plated ZTA was used, the surface roughness of sample F10-2 was the lowest, while sample F10-5 is the lowest after electroless nickel plating. The reason is that part of the ZTA particles in the F10-2 Cu-ZTA cermet will break and flake during the grinding process, resulting in only contact between the binder and the sample, thus obtaining a better machining surface. However, due to the high content of Cu binder, ZTA particles are wrapped in binder in the sample F10-5, and the contact area between ZTA and the steel bars is small. Therefore, the processed surface is good, and the low abrasion loss of sample F10-5 to steel bars also supports this conclusion. Comparing samples F10-5 and F14-2 to analyze the effect of ZTA particle size on the surface roughness of steel bars, the study found that as the particle size of ZTA decreases, the surface roughness of the steel bar increases slightly. Comparing samples F14-2 and F14 + 16−1, it can be found that as the particle size of ZTA particles is further reduced, the surface roughness of the steel bar is greatly reduced. Therefore, the roughness of the ground surface can be improved by reducing the particle size of the ZTA particles.

In summary, during the grinding process, it was found that with the increase of the binder content, the removal rate of the material increased and the surface roughnessdecreased. Under the condition of the same binder content, when the ZTA particle size decreases, the removal rate of Cu-ZTA cermet increases, and the surface roughness of steel bar is reduced. This conclusion is consistent with the results of Gao *et al* [63].

3.7. Analysis of wear behavior of Cu-ZTA cermet

Figure 9 is a schematic view of the wear behavior of Cu-ZTA cermets during grinding. The wear properties of cermets are mainly affected by the hardness of the matrix, the bonding ability of the bonding agent, and the strength of the ceramic phase [64, 65]. The grinding process is shown in figures 9(a)–(f). Figures 9(a) and (d) are initial state of Cu-ZTA cermet. Figures 9(b) and (c) are the schematic diagram of grinding process. Under

loading conditions, the ZTA particles contact with the surface of the steel bar. Under the action of the tangential force, the abrasive wear of ZTA particles will take place (figure 9 (e)). As the grinding process progresses, the attrition rate of ZTA particles increased. In figures 4(b) and (c), it can be clearly seen that there is a distinct interfacial layer between the ZTA and the Cu matrix. This porous interface layer breaks up during high-speed grinding due to increased loading, causes the extraction of ZTA particles (figure 9(f)). The grain drawing phenomenon is mainly caused by bond fracture or bond interface fracture [66]. In addition, when the ZTA particles are all worn to a very low protrusion height, or part of the ZTA particles are pulled out during the grinding process, the Cu binder also participates in the grinding process and remains on the surface of the steel bar [66].

4. Conclusions

In this paper, Cu-ZTA cermets with different content of binder and different particle size ZTA particles were prepared by powder metallurgy, and the following conclusions can be obtained:

1. Electroless nickel plating can significantly improve the bonding ability between ZTA particles and Cu matrix, and the electroless nickel-plated Cu-ZTA cermet has a higher material removal rate.
2. Vacuum hot pressing sintering increases the density of Cu-ZTA cermets. The addition of alloying elements can form Cu solid solution. The best friction and wear properties of Cu-ZTA cermets with 35% Cu binder and ZTA particle size F14/F16. The micro Vickers hardness is 192.04 ($\pm$14) $HV_{0.1}$, the grinding ratio is 1.927, the friction coefficient is 0.508, and the surface roughness of the machined surface is 25.092 μm.
3. There are two interfacial layers between ZTA and Cu matrix. One interface is that Cu atoms replace Ni atoms during hot pressing, which improves the bonding ability between Cu and ZTA. The Cu/ZTA interface is a mechanical bonding interface. The other interface is the interface of Cu_3Ti_3O and TiO_x formed by the reaction of Al_2O_3 with Ti in the matrix, and the interface is a reaction bonding interface.
4. The failure of Cu-ZTA cermet is mainly due to the occurrence of ZTA wear, fracture and extraction at the Cu/ZTA interface. Stress concentration at the interface under load, and the microcracks generally originate at the interface. As the load increases, the cracks continue to expand until the fracture and ZTA granularity are pulled out, causing the failure of Cu-ZTA cermet .

Acknowledgments

This work was funded by Key Laboratory of Infrared Imaging Materials and Detectors, Shanghai Institute of Technical Physics, Chinese Academy of Sciences (No. IIMDKFJJ-17-06), Sichuan Science and Technology Support Program (No. 2016FZ0079), National Natural Science Foundation of China (No. 51201143), China Postdoctoral Science Foundation (No. 2015M570794, No. 2018T110993), R&D Projects Funding from the Research Council of Norway (No. 263875/H30).

ORCID iDs

Xiao-song Jiang https://orcid.org/0000-0002-6703-9116

References

[1] Franco E, da C, César E, Tsipas S A and Gordo E 2015 Cermets based on FeAl–NbC from composite powders: Design of composition and processing *Int. J. Refract. Met. H.* **48** 324–32
[2] Pan Y F, Liu A J, Huang L, Du Y, Jin Y Q, Yang X Y and Zhang J X 2019 Effects of metal binder content and carbide grain size on the microstructure and properties of SPS manufactured WC-Fe composites *J. Alloy. Compd.* **784** 519–26
[3] Wang Z, Lin T, He X B, Shao H P, Zheng J S and Qu X H 2015 Microstructure and properties of TiC-high manganese steel cermet prepared by different sintering processes *J. Alloy. Compd.* **650** 918–24
[4] Peng Y, Miao H and Peng Z 2013 Development of TiCN-based cermets: Mechanical properties and wear mechanism *Int. J. Refract. Met. H.* **39** 78–89
[5] Rajabi A, Ghazali M J, Syarif J and Daud A R 2014 Development and application of tool wear: a review of the characterization of TiC-based cermets with different binders *Chem. Eng. J.* **255** 445–52
[6] Ji W B, Zou B, Liu Y N, Huang C M and Guo P 2017 Frictional behavior and wear resistance performance of gradient cermet composite tool materials sliding against hard materials *Ceram. Int.* **43** 7816–26
[7] Smith L M, Averill R C, Lucas J P, Stoughton T B and Matin P H 2003 Influence of transverse normal stress on sheet metal formability *Int. J. Plasticity.* **19** 1567–83
[8] Wang J, Zheng K H and Zhou N 2013 Influence of Ni coating on the interface performance of Al/ZTA *Rare. Metal. Mat. Eng.* **42** 280–2

[9] Rostami R B and Tajally M 2014 Improvements in microstructure and mechanical properties of Al–Si–Cu alloy–Al_2O_3 nanocomposite modified by ZrO_2 *J. Mater. Res.* **29** 2505–13
[10] Feng Q, Duan X Z, Dong B X and Yang H Y 2018 Effects of Cr and Zr addition on microstructures, compressive properties, and abrasive wear behaviors of *in situ* TiB_2/Cu cermets *Materials.* **11** 1464
[11] Janas D and Liszka B 2017 Copper matrix nanocomposites based on carbon nanotubes or graphene *Mater. Chem. Front.* **10** 1039
[12] Hong C Q, Han J C, Zhang X H and Meng S H 2007 Influence of hot pressing on microstructure and mechanical properties of combustion synthesized TiB_2-Cu-Ni composite *J. Mater. Process. Tech.* **183** 445–9
[13] Shabani M, Paydar M H, Zamiri R, Goodarzi M and Moshksar M M 2015 Microstructural and sliding wear behavior of SiC-particle reinforced copper matrix composites fabricated by sintering and sinter-forging processes *J. Mater. Res. Technol.* **5** 5–12
[14] Ru J J, Jiang Y H, Zhou R and Feng J 2017 Preparation of Ni-encapsulated ZTA particles as precursors to reinforce iron-based composites *Adv. Eng. Mater.* **19** 1700268
[15] Ru J J, He H, Jiang Y H and Zhou R 2019 Wettability and interaction mechanism for Ni-modified ZTA particles reinforced iron matrix composites *J. Alloy. Compd.* **786** 321–9
[16] Zhao H W, Li J H, Guo S B, Fan D D, Liu G H and Li J T 2017 Fast preparation of ZTA-TiC-FeCrNicermets by high-gravity combustion synthesis *Ceram. Int.* **43** 6904–9
[17] Dent A H, Depalo S and Sampath S Examination of the wear properties of HVOF sprayed nanostructured and conventional WC-Co cermets with different binder phase contents *J. Therm. Spray. Techn.* **11** 551–8
[18] Naga S M, El-Maghraby H F, Mand E and Saleh M A 2018 Characterization and origin of failure of SiC/ZTA composites *Int. J. Refract. Met. H.* **73** 53–7
[19] Zhou M J, Sui Y D, Chong X Y and Jiang Y H 2018 Wear resistance mechanism of ZTAP/HCCI composites with a honeycomb structure *Metals-Basel.* **8** 5–88
[20] Fan L, Wang Q, Yang P, Chen H H, Hong H P, Zhang W T and Ren J 2018 Preparation of nickel coating on ZTA particles by electroless plating *Ceram. Int.* **44** 11013–21
[21] Bolelli G, Lusvarghi L and Barletta M 2009 HVOF-sprayed WC–CoCr coatings on Al alloy: effect of the coating thickness on the tribological properties *Wear* **26** 7944–53
[22] Barletta M, Bolelli G, Bonferroni B and Lusvarghi L 2010 Wear and corrosion behavior of HVOF-sprayed WC-CoCr coatings on Al alloys *J. Therm. Spray. Techn.* **19** 358–67
[23] Ru J J, He H, Jiang Y H, Zhou R and Hua Y X 2019 Ionic liquid-assisted preparation of Ni–Cr Dual WRAPPEDZTA particles for reinforced iron-based composites *Adv. Eng. Mater.* **21** 1801120
[24] Simunkova H, Pessenda-Garcia P, Wosik J, Angerer P, Kronberger H and Nauer G E 2009 The fundamentals of nano- and submicro-scaled ceramic particles incorporation into electbareposited nickel layers: Zeta potential measurements *Surf. Coat. Tech.* **203** 1806–14
[25] Liao J, Jian C L and Kuo K H 1989 A TEM study of CVD TiC_x /$Ti(C, N)_x$ coating on WC-Co cemented carbide *Metall. Mater. Trans. A* **20** 279–85
[26] Zhou M, Bi H, Lin T Q, Lv X J, Wan D Y, Huang F Q and Lin J H 2014 Heat transport enhancement of thermal energy storage material using graphene/ceramic composites *Carbon* **75** 314–21
[27] Meng J P, Fu Z Q, Liu X P, Yue W and Wang C B 2014 Influence of ion/atom arrival ratio on structure and optical properties of AlN films by ion beam assisted deposition *Appl. Surf. Sci.* **31** 7760–4
[28] Leon C A and Drew R A L 2000 Preparation of nickel-coated powders as precursors to reinforce MMCs *J. Mater. Sci.* **35** 4763–8
[29] León C A and Drew R A L 2002 The influence of nickel coating on the wettability of aluminum on ceramics *Compos. Part. A-Appl. S.* **33** 0–1432
[30] Hao L, Wei J and Gan F X 2009 Electroless Ni–P coating on W–Cu composite via three different activation processes *Surf. Eng.* **25** 72–375
[31] Xu H, Zhang C B, Wang Z K, Ding D L, Wang W J, Xu T Y and Liu H 2017 Research progress of pretreatment process for electroless nickel plating on magnesium alloy surface *Surf. Technol.* **46** 87–94
[32] Belov N A 2010 Quantitative phase analysis of the Al–Zn–Mg–Cu–Ni phase diagram in the region of compositions of high-strength nickalines *Russ. J. Non-Ferr. Met.* **51** 243–9
[33] Jiang X S, Song T F, Shao Z Y, Liu W X, Zhu D G and Zhu M H 2017 Synergetic effect of graphene and MWCNTs on microstructure and mechanical properties of Cu/Ti_3SiC_2/C nanocomposites *Nanoscale Res. Lett.* **12** 607
[34] Ibrahim A E A M and Kim H S 2018 Effect of the fabrication method on the wear properties of copper silicon carbide composites *Tribol. Int.* **128** 140–54
[35] Ji W B, Zou B, Huang C Z, Liu Y N and Huang C M 2017 Fabrication, microstructure and mechanical properties of self-diffusion gradient cermet composite tool materials *Mat. Sci. Eng. A-Struct.* **685** 332–41
[36] Gu K K, Lin Q, Wang W J, Wang H Y, Guo J, Liu Q Y and Zhu M H 2015 Analysis on the effects of rotational speed of grinding stone on removal behavior of rail material *Wear* **342–343** 52–9
[37] Azimi A, Shokuhfar A and Zolriasatein A 2014 Nanostructured Al–Zn–Mg–Cu–Zr alloy prepared by mechanical alloying followed by hot pressing *Mat. Sci. Eng. A-Struct.* **595** 124–30
[38] Varol T and Ozsahin S 2017 Artificial neural network analysis of the effect of matrix size and milling time on the properties of flake Al-Cu-Mg alloy particles synthesized by ball milling *Particul. Sci. Technol.* **23** 381–90
[39] Jiang X S, Liu W X, Li Y J, Shao Z Y, Luo Z P, Zhu D G and Zhu M H 2017 Microstructures and mechanical properties of Cu/Ti_3SiC_2/C/graphene nanocomposites prepared by vacuum hot-pressing sintering and hot isostatic pressing *Compos. Part. B-Eng.* **141** 203–13
[40] Choi H J, Shin J H and Bae D H 2012 The effect of milling conditions on microstructures and mechanical properties of Al/MWCNT composites *Compos. Part. A-Appl. S.* **43** 1061–72
[41] Yue H Y, Yao L H, Gao X, Zhang S L, Guo E J, Zhang H, Lin X Y and Wang B 2017 Effect of ball-milling and graphene contents on the mechanical properties and fracture mechanisms of graphene nanosheets reinforced copper matrix composites *J. Alloy. Compd.* **691** 755–62
[42] Koppad P G, Ram H R A, Ramesh C S, Kashyap K T and Koppad R G 2013 On thermal and electrical properties of multiwalled carbon nanotubes/copper matrix nanocomposites *J. Alloy. Compd.* **580** 527–32
[43] Hwang H J, Nagai T, Ohji T and Sando M 1998 Curie temperature anomaly in lead zirconatetitanate/silver composites *J. Am. Ceram. Soc.* **81** 709–12
[44] Pecharroman C, Betegon F E, Eartolome J F and Esteban S L 2001 New percolative $BaTiO_3$ –Ni composites with a high and frequency-independent dielectric constant ($\varepsilon r = 80{,}000$) *J. Adv. Mater.* **13** 1541–4

[45] Wakashima K, Choi B H and Mori T 1990 Plastic incompatibility and its accommodation by diffusional flow: modelling of steady state creep of a metal matrix composite *Mat. Sci. Eng. A-Struct.* **127** 57–64
[46] Mamivand M, Zaeem M A and Kadiri H E 2014 Phase field modeling of stress-induced tetragonal-to-monoclinic transformation in zirconia and its effect on transformation toughening *Acta Mater.* **64** 208–19
[47] Basu B 2005 Toughening of yttria-stabilised tetragonal zirconia ceramics *Int. Mater. Rev.* **50** 239–56
[48] Ramos M I, Suguihiro N M, Brocchi E A, Navarro R and Solorzano I G 2017 Microstructure investigation of Cu-Ni base Al_2O_3 nanocomposites: from nanoparticles synthesis to consolidation *Metall. Mater. Trans. A* **48** 2643–53
[49] Zhou J M, Zhu D G, Tang L T, Jiang X S, Chen S, Peng X and Hu C F 2016 Microstructure and properties of powder metallurgy Cu-1% Cr-0.65%Zr alloy prepared by hot pressing *Vacuum* **131** 156–63
[50] Fu H D, Xu S, Li W, Xie J X, Zhao H B and Pan Z J 2017 Effect of rolling and aging processes on microstructure and properties of Cu-Cr-Zr alloy *Mat. Sci. Eng. A-Struct.* **700** 107–15
[51] Van Nguyen C, Deng Y, Bezold A and Broeckmann C 2016 A combined model to simulate the powder densification and shape changes during hot isostatic pressing *Comput. Method. Appl. M.* **315** 302–15
[52] Cao J Y, Xiao P A, Dai K L, Li C K and Zhang X 2014 Thermal dehydrogenation behavior of TiH_2 and its dynamics calculation *T. Nonferr. Metal. Soc.* **24** 733–8
[53] Wang X Y, Li C, Si X Q, Qi J L, Feng J C and Cao J 2018 Brazing ZTA ceramic to TC4 alloy using the Cu foam as interlayer *Vacuum* **155** 7–15
[54] Voytovych R, Robaut F and Eustathopoulos N 2006 The relation between wetting and interfacial chemistry in the CuAgTi/alumina system *Acta Mater.* **54** 2205–14
[55] Shiue R K, Wu S K J M O and Wang J Y 2000 Microstructural evolution at the bonding interface during the early-stage infrared active brazing of alumina *Metall. Mater. Trans. A* **31** 2527–36
[56] Durov A V, Naidich Y V and Kostyuk B D 2005 Investigation of interaction of metal melts and zirconia *J. Mater. Sci.* **40** 2173–8
[57] Kozlova O, Braccini M, Voytovych R, Eustathopoulos N, MartinettiP and Devismes M-F 2010 Brazing copper to alumina using reactive CuAgTi alloys *Acta Mater.* **58** 1252–60
[58] Ramkumar K R, Sivasankaran S and AlaboodiA S 2017 Effect of alumina content on microstructures, mechanical, wear and machining behavior of Cu–10Zn nanocomposite prepared by mechanical alloying and hot-pressing *J. Alloy. Compd.* **709** 129–41
[59] Mechnik V A, Bondarenko N A, Dub S N and Kolodnits'kyi V M 2018 A study of microstructure of Fe–Cu–Ni–Sn and Fe–Cu–Ni–Sn–VN metal matrix for diamond containing composites *Mater. Charact.* **146** 209–16
[60] Song D D, Wan L, Liu X P, Hu W D, Xie D L and Wang J S 2016 Effect of hot pressing temperature on microstructure, mechanical properties and grinding performance of vitrified-metal bond diamond wheels *Int. J. Refract. Met. H.* **54** 289–94
[61] Lin B, Zhou K, Guo J, Liu Q Y and Wang W J 2018 Influence of grinding parameters on surface temperature and burn behaviors of grinding rail *Tribol. Int.* **122** 151–62
[62] Wang W J, Gu K K, Zhou K, Cai Z B, Guo J and Liu Q Y 2018 Influence of granularity of grinding stone on grinding force and material removal in the rail grinding process *P. I. Mech. Eng. J-J. Eng.* **233** 355–65
[63] Gao S, Kang R K, Dong Z G, Zhang B and Wang Z G 2016 Surface integrity and removal mechanism in grinding sapphire wafers with novel vitrified bond diamond plates *Mater. Manuf. Process.* **32** 121–6
[64] Li Q, Li Z H, Tan H Y, Feng D D and Zhu Y M 2016 Comparison of Cu and Zn on properties of vitrified diamond composites *Diam. Relat. Mater.* **66** 217–22
[65] Miao Q, Ding W F, Fu D K, Chen Z Z and Fu Y C 2017 Influence of graphite addition on bonding properties of abrasive layer of metal-bonded CBN wheel *Int. J. Adv. Manuf. Tech.* **93** 1–10
[66] Li Z, Ding W F, Ma C Y and Xu J H 2015 Grinding temperature and wheel wear of porous metal-bonded cubic boron nitride superabrasive wheels in high-efficiency deep grinding *P. I. Mech. Eng. B-J. Eng.* **231** 1961–71